Smart Films Produced by Electrospinning of Poly(butylene-adipate-*co*-terephthalate)/poly-(ε-caprolactone) for Controlled Delivery of Ibuprofen

Janice C. Hardt,[a] Gabriel N. Fraga,[a,b] Alessandra R. Medeiros, [a,b] Ariane R. S. Rossin,[a,b]
Josiane Caetano,[a] Matheus C. O. Leite,[c] Bruno V. L. da Fonseca,[c] Bruno H. Vilsinski [*,c]
and Douglas C. Dragunski [*,a,b]

[a]Grupo Interdisciplinar de Fotoquímica e Eletroquímica Ambiental,
Centro de Engenharias e Ciências Exatas, Universidade Estadual do Oeste do Paraná,
85903-000 Toledo-PR, Brazil

[b]Departamento de Química, Universidade Estadual de Maringá, 87020-900 Maringá-PR, Brazil

[c]Grupo de Materiais Biopoliméricos e Compósitos (GMBC), Universidade Federal de Juiz de Fora,
36036-900 Juiz de Fora-MG, Brazil

Wound dressing devices composed of microfibers of poly(butylene-adipate-*co*-terephthalate) and poly-(ε-caprolactone) incorporated with ibuprofen were obtained by electrospinning technique. The effect of ibuprofen concentration (0, 10, and 20% m m^{-1}) on morphology, spectroscopic, and thermal characterization was evaluated. The fibers containing ibuprofen presented beads and revealed no uniformity. The spectroscopic analysis showed signals that reveal the ibuprofen incorporation on fibers. At the same time, X-ray diffraction spectroscopy indicated a difference in the fiber crystallinity depending on drug concentration, where a lower crystallinity was verified by the film containing a greater concentration incorporated. Rheological measurements revealed that films were more plastic in greater ibuprofen incorporation. Contact angle characterization revealed that ibuprofen solubilization on composite surfaces increased the film wettability. Finally, the fibers promoted the controlled release of ibuprofen, promoting morphological changes in polymeric matrices. The material developed can be used in future biomedical applications.

Keywords: PBAT, PCL, ibuprofen, electrospinning

Introduction

Ibuprofen (IBU, [(*RS*)-2-(4-(2-methyl propyl)phenyl) propanoic acid) is a known anti-inflammatory drug non-steroidal used against fever, pain, and symptoms of rheumatoid, arthritis, and osteoarthritis.[1,2] Besides its broad uses, its low solubility (49 µg mL^{-1} at 25 ºC), rapid clearance after oral administration, and short half-life (2 h) are the main drawbacks associated with this molecule.[1,2] IBU also presents poor skin permeability, making its transdermal application more difficult.[1] This requires high and multiple dosages in patients, generating several side effects, such as bleeding and ulceration.[1,2] Researchers have been developing transdermal and topical formulations of IBU to overcome these drawbacks, increase therapeutic efficacy, and improve patient adherence. Several drug delivery systems have been used to solubilize and promote the controlled drug delivery of IBU, such as β-cyclodextrin, lipid carriers, hydrogels, microemulsions, surfactants, mesoporous silica, etc.[1-3] Notably, IBU has been incorporated in formulations containing skin penetration enhancers for transdermal controlled release, such as ethanol 70%. However, these systems promote skin irritation and lead to quick evaporation, limiting their use.[1] It is increasing the studies involving the obtention of microfibers as drug carriers, mainly due to their better patient compliance, higher encapsulation efficiency, reduced heterogeneity of therapeutic concentration of the drug in the carrier, etc.[4]

Electrospinning is one of the most used methods to produce fibers with diameters varying from micro to nanometers.[5] These fibers can be used in biomedical applications, such as wound healing, tissue engineering scaffolds, enzyme immobilization, and drug delivery

systems.[6,7] Generally, the fibers obtained by electrospun present a high surface area, allowing the *in situ* incorporation of bioactive agents alongside variable porosity and morphologies similar to extracellular matrix structure (ECM).[5,8] Poly(butylene-adipate-*co*-terephthalate) (PBAT) is a polyester derived from fossil sources that presents interesting properties for biomedical materials, such as biodegradability, toughness, and high flexibility.[8] Additionally, it offers high processability, high elongation at break, and mechanical properties similar to a thermoplastic elastomer. It is a bioplastic candidate to replace synthetic polymers in several applications, such as packaging, agricultural, and biomedical.[4,9] However, it is also worth mentioning that the low elastic modulus PBAT, as well as its poor oxygen barrier properties, is a disadvantage for using only this polymer in the materials.[10] Polycaprolactone (PCL) is a polymer approved by Food and Drug Administration (FDA) that has been extensively used in bone regeneration, as well as to obtain materials for tissue engineering purposes due to its mechanical elasticity and low autoimmune response.[11] However, the main disadvantage of the PCL is its surface hydrophobicity, which exerts a direct influence on cell attachment and proliferation.[12] In this way, our research group has combined PBAT with PCL to obtain materials with better performance for biomedical applications.[9]

Rizvi and D'Souza[13] reported the electrospinning of PBAT/PCL for use in drug delivery systems. The authors believe in the potential of the union of these polymers due to their biodegradable and biocompatible characteristics. Aiming for a more advanced application, the electrospinning of PBAT/PCL together with propolis for dressings has already been reported by Zanella *et al.*[14] with satisfactory results for antimicrobial activity. Recently, we studied the synthesis and characterization of a wound dressing device composed of monoaxial electrospun PBAT/PCL-based microfibers incorporated with silver sulfadiazine (SS).[4] Fibers presented diameters varying from 3.113 (without PCL) to 0.591 μm (10% of PCL m m⁻¹).[4] Thermal stability studies revealed that SS incorporation presented a low influence over the degradation temperature of fibers. SS increased the fiber's crystallinity, and the final material was effective against Gram-negative and Gram-positive bacteria (*Escherichia coli* and *Staphylococcus aureus*, respectively).[4] Finally, this article incorporated IBU, a drug with different polarity degree, and subsequent characterization of the PBAT/PCL/IBU fibers. The main difference of the present study is that IBU is soluble in the same solvents used to obtain fibers (chloroform), while SS is not. The fiber's main characteristics were compared with the previous article.[4]

Experimental

Materials

Poly-(ε-caprolactone) (PCL, 65.000 g mol⁻¹) was obtained from Sigma-Aldrich (São Paulo, Brazil). Poly(butylene-adipate-co-terephthalate) (PBAT, 65.000 g mol⁻¹) was acquired from BASF with the commercial name ECOFLEX® (São Paulo, Brazil). Organic solvents chloroform (CHCl₃ 99%) and *N*-dimethylformamide (DMF, C₃H₇NO) were acquired from FMaia (São Paulo, Brazil) and Neon Commercial (Belo Horizonte, Brazil), respectively. The drug ibuprofen ($C_{13}H_{18}O_2$, IBU, purity degree of 99%) was obtained from the Prati-Donaduzzi (Toledo, Brazil) pharmaceutical industry.

Methods

Polymeric solution preparation

The preparation of the polymeric solution at 20% (m v⁻¹) occurred by using PCL 25% (m m⁻¹) and PBAT 75% (m m⁻¹) to obtain 5.0 mL of the final solution. It involves using 0.75 and 0.25 g of PBAT and PCL, respectively. According to a previous study,[4] this proportion of polymers results in thin and homogeneous fibers. The solvent quantities were added in the following steps to obtain 85 and 15% (v v⁻¹) of chloroform (Chl) and dimethylformamide (DMF), respectively. The solution was magnetically stirred for 24 h. DMF presents a higher dielectric constant than chloroform at 25.0 °C, favoring electrospinning.[15]

Ibuprofen incorporation

The working concentration chosen for IBU was 20 and 30% in relation to the mass of the PBAT/PCL blend, being designated PBAT/PCL-20 and PBAT/PCL-30, respectively. For incorporation, IBU was added to the PBAT/PCL solution and stirred until complete dissolution. Afterward, 5.0 mL of the final solution was transferred to a graduated glass syringe (10.0 mL) containing a needle (internal diameter of 0.7 mm) and put in an infusion pump system. The negative pole is connected to the target collector and an alternating cable. The positive pole is positioned to the needle. We used the following electrospinning conditions for the systems containing or not IBU: needle-to-connector distance of 12 cm, a potential voltage applied of 15 kV, flow rate of 1.0 mL h⁻¹, temperature of 23.5 ± 1.5 °C, and relative air humidity of 50 (± 5)%.

Solution characterization

Relative viscosity (η_{rel}) was measured using an Ubbelohde capillary viscometer (MyLabor, No. 300, São

Paulo, Brazil). Measurements were carried out with a viscometer immersed in a water bath at 23 ± 2 °C. The solutions were glued to the viscometer and left to rest until they reached the bath temperature. Flow times were performed in triplicate for each sample.

The conductivity of the solutions was evaluated using an MS TECNOPON conductivity meter (model mCE-105, Piracicaba, Brazil) with a measurement range of 0 to 200 mS cm^{-1}, cell constant (K) of 1 ± 0.2, resolution of 0.1 μS cm^{-1}, and electrode area of 140 mm × (Ø) 10 mm. The temperature of the measurement solutions was 25 ± 3 °C. The assay was performed in triplicate.

Membranes characterization

The fiber morphology was evaluated by scanning electron microscopy (SEM) using a microscope model VEGA3 TESCAN (Kohoutovice, Czech Republic). Briefly, the samples were fixed in the support through a carbon adhesive tape and gold metalized through a Denton Vacuum (Desk V) metallizer (Moorestown, USA) (thickness of 5 nm). The analysis was performed at 20 kV.

The fiber's wettability was evaluated using the sessile drop method. The samples were placed in a metal plate, where distilled water (ca.7 μL) was deposited into the fibers. The contact angle was measured through analysis of the images through the software AmScope 3.7 (Irvine, USA).

The IBU incorporation was evaluated by Fourier transformed infrared spectroscopy (FTIR) using the attenuated total reflectance (ATR) module. These analyses were performed using a PerkinElmer FTIR Spectrometer (Waltham, USA). The measures were performed in the wavelength range from 4000 to 650 cm^{-1} at 25 °C, using eight scans (resolution of 1 cm^{-1}).

The X-ray diffraction was used to evaluate the crystallinity change after IBU incorporation in fibers. A Bruker™ Diffractometer (Billerica, USA) realized this analysis at a diffraction angle (2θ) ranging from 4 to 60° (resolution of 0.01). A radiation source of Cu Kα (λ = 1.5406 Å) and a graphite monochromator were used in the analysis.

Differential scanning calorimetry (DSC) and thermogravimetric analysis were used to characterize the thermal behavior of the fibers without and containing IBU. In DSC analysis, the samples (5.940 ± 0.6200 mg) were placed in closed aluminum crucibles under a nitrogen atmosphere (flow rate of 50 mL min^{-1}). The samples were heated and cooled from 25 to 200 °C (at 10 °C min^{-1}). The crystallinity percentage (x_c) of the fibers was obtained using equation 1:

$$x_c = \left(\frac{\Delta H_m}{\Delta H_m^0 \left(1 - \dfrac{wt.\%}{100} \right)} \right) \times 100 \qquad (1)$$

where ΔH_m and ΔH_m^0 are the melting and theoretical melting enthalpies, respectively. ΔH_m^0 is defined as the enthalpy of a sample 100% crystalline (114 and 139 J g^{-1} for PBAT and PCL, respectively).[4] Thermogravimetric analyses were obtained to evaluate the degradation temperature of fiber containing or no IBU. Thermograms were obtained by a PerkinElmer STA 6000 Thermal Analyzer (Waltham, USA). The samples (average mass around 7.291 ± 1.339 mg) were put in porcelain crucibles using the same conditions discussed in DSC.

Mechanical tensile-strength analyses were obtained for the films. For this, the stress-strain curves were obtained, following the ASTM-D882-12[16] technical standard, using a texturometer TA HD Plus (Stable Micro Systems) with 5 kg of the load cell (Vienna Court, UK). The analysis was performed in triplicate until the films were utterly broken, with a traction ratio of 1 mm s^{-1} and 10 mm.

Release kinetics

The IBU release kinetics were obtained in 100.0 mL of phosphate buffer (pH 7.4) at 0.10 mol L^{-1} and 37.0 °C. This media simulates the pH and temperature of the skin. First, an analytic curve for different IBU concentrations was obtained by SHIMADZU UV-Vis spectrophotometer, UV-1800 (Kyoto, Japan) at 264 nm. The IBU release studies from fibers were used in a controlled bath shaker Newlab NL-343-01 (Piracicaba, Brazil) at 100 rpm and controlled temperature (37 ± 2 °C). The amount of IBU released was evaluated by UV-Vis using solutions aliquots (2.0 mL) in different time intervals. In each time interval, the same medium quantity was replaced in the systems to maintain a constant volume.

The initial IBU concentration incorporated in fibers was evaluated using an analytical curve in ethanol. For this, 10.0 mg of IBU films were solubilized in 5.0 mL of ethanol for 2 h, and the amount of IBU incorporated was evaluated through the absorbance at 264 nm.

The release curves were fitted using different release models, such as zero and first orders, Higushi, Korsmeyer-Peppas, Hixson-Crowell, Hopfenberg, Baker-Lonsdale, Peppas-Sahlin, Quadratic, Weibull, Gompertz, and Probit. These models predict the mechanism of the IBU release from fibers. The fitting was obtained using DDSolver software using a non-linear optimization method.[17] Finally, we used the correlation coefficient (R^2) and the Akaine

Information Criterion (AIC) to evaluate the best-fitting model.[18,19]

The same characterizations performed by PBAT/PCL/IBU films were also carried out for the samples after the IBU release reached equilibrium. In this way, films after 1500 min in contact with phosphate buffer solution (PBS) were dried and performed to the measurements.

Results and Discussion

Solution characterization

The PBAT/PCL solution (Table 1) has a conductivity very close to the binary mixture Chl/DMF (1.206 ± 0.004 µs cm^{-1}), indicating a neutral characteristic of the polymers in the solution. The addition of IBU causes a decrease in the conductivity of the solution with increasing concentration, resulting from the presence of IBU in anionic form. In solution, IBU can have a neutral or anionic form depending on the pH of the medium.[20] Sequeira *et al.*[21] also observed a reduction in conductivity with the addition of IBU to poly(vinyl alcohol)/lysine solution for electrospinning.

Table 1. Conductivity and viscosity determined for electrospun solutions

Solution	Conductivity / (µs cm^{-1})	Relative viscosity
PBAT/PCL	1.17 ± 0.023	4.044 ± 0.095
PBAT/PCL/IBU-20	1.011 ± 0.0066	2.983 ± 0.023
PBAT/PCL/IBU-30	0.828 ± 0.016	2.985 ± 0.045

PBAT: poly(butylene-adipate-*co*-terephthalate); PCL: poly-(ε-caprolactone); IBU: ibuprofen.

Table 1 also shows the relative viscosities of the studied solutions. The relative viscosity of the PBAT/PCL blend is reduced with the addition of IBU and can be eliminated by the interaction of the polymer-IBU. Khan *et al.*[22] reported that IBU has an intermediate interaction with neutral polymers that can cause changes in the solution. Furthermore, IBU is a known drug with a plasticizing characteristic that causes a decrease in viscosity.[23]

General characterization of PBAT/PCL/IBU films

Figure 1 presents the SEM images of PBAT/PCL with, and without IBU incorporation.

First, PBAT/PCL fibers were uniform and continuous, without bead formation (Figures 1a and 1d). SEM images reveal that IBU incorporation significantly changes the morphology of the fibers. SEM images (Figures 1b, 1c and 1f) show beads' formation without presenting uniformity. The reduction in viscosity by approximately 30%, shown in Table 1, may explain the significant formation of beads. The formation of beads is related, among other factors, to the solution viscosity parameter. The reduction in the viscosity of a solution leads to the formation of beads or electrospraying.[24] For PBAT/PCL/IBU-30, it is impossible to observe any fibers formed. This fact can be explained by the reduction in the conductivity of the solution presented in Table 1. Conductivity can influence the formation of smooth fibers due to the density of charges present in the solution that interfere with the stability of the formed jet.[24]
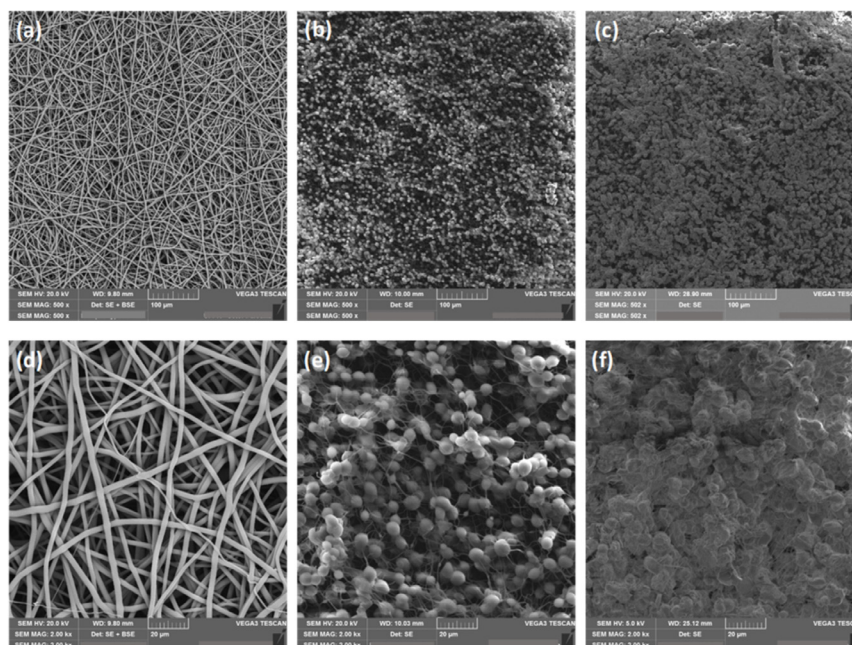

Figure 1. SEM images of PBAT/PCL films at (a) 500×, (d) 2000×, PBAT/PCL-20 at (b) 500×, (e) 2000×, and PBAT/PCL-30 at (c) 500×, and (f) 2000×.

Figure 2 presents the FTIR spectra of the films studied. The IBU FTIR spectra reveal the presence of the following bands: 2924 (hydrogen atoms axial deformation at primary carbon-CH$_3$), 1419, and 1321 (axial deformation of C−O of the carboxylic acid group), 936 (angular deformation out of the plane of C=O binding), and 779 cm^{-1} (angular deformation of hydrogens of the *para*-substituted aromatic ring).[25] All these vibrational modes are found in the FTIR spectra of PBAT/PCL/IBU films, which indicates the IBU incorporation in the polymeric matrices. Finally, the broadband at the wavelength ranges from 2900 to 3400 cm^{-1} present only in the IBU FTIR spectra due to the carboxylic acid present in this drug. The band at 1269 cm^{-1} is also observed in the FTIR spectra of the pure polymers and the films containing IBU. However, in the last, an increase in intensity is observed due to the overlap of ester C−O bands of PBAT with C−O carboxylic acid of IBU.
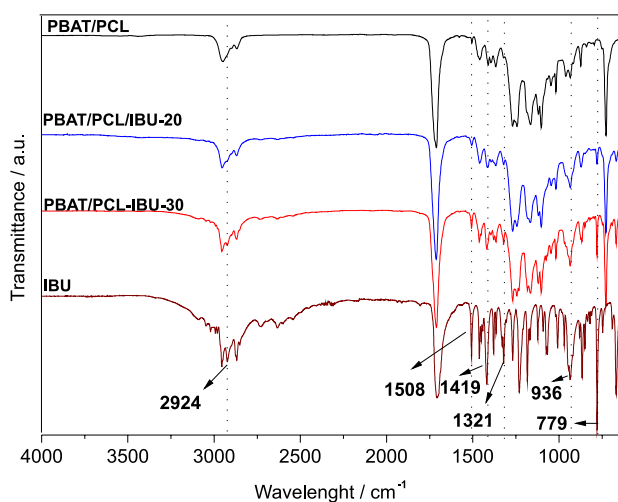

Figure 2. FTIR-ATR spectra of PBAT/PCL films without and with IBU incorporation at different concentrations.

Mechanical analyses were performed to investigate this possibility better (Figure 3).

The tensile strength curves reveal that the films containing 30% (m m^{-1}) of IBU presented higher tensile strength, indicating a behavior of less plastic for this sample (Figure 3). The tensile strength of films was 1.60, 0.08, and 0.49 MPa for the samples PBAT/PCL, PBAT/PCL/IBU-20 IBU, and PBAT/PCL/IBU-30, respectively. These results also indicate a higher crystallinity for the lower IBU concentration film. Finally, it is necessary to mention that IBU incorporated the lowest strength of the films. The characteristic of IBU can explain this to act as a plasticizer.[26] Plasticizers can disrupt the polymeric network and, consequently, reduce tensile strength due to the greater flexibility of the material.[27] IBU incorporation decreases the intermolecular polymeric chain interactions between
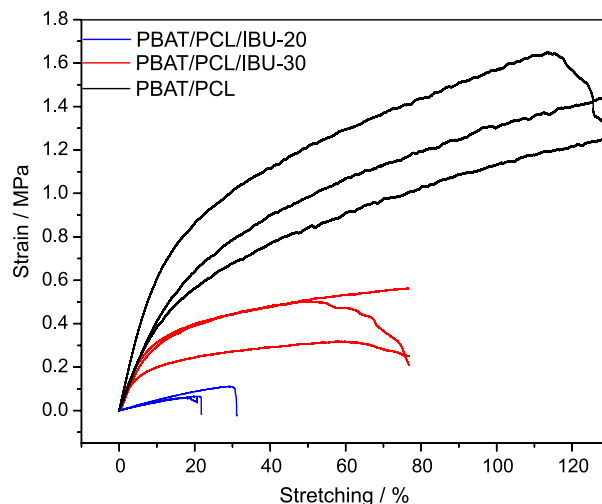

Figure 3. Strain-stretching curves of PBAT/PCL films (black), PBAT/PCL/IBU-20 IBU (blue), and PBAT/PCL/IBU-30 IBU (red).

PBAT and PCL.[28] However, it is necessary to mention that the mechanical behavior presented here did not compromise using PBAT/PCL/IBU films for biomedical purposes.[28] Jin *et al.*[28] discussed that materials with higher crystallinity offer high elastic moduli and resistance to tensile force. It directly compromises the ductility of the fiber for transdermal application, harming its use.[28] However, our electrospun matrices presented tensile strength values in accordance with materials which has been applied to wound healing *in vivo* study.[28]

X-ray diffraction analysis was performed to investigate better the crystallinity behavior of the films (Figure 4). The peak characteristics for the films containing IBU were in 2θ angles of 12.4, 16.7, 20.3, and 22.5°. These peaks are present in IBU, as previously reported by Yu *et al.*[29] The peak 2θ located at 17.5° presented in the diffractogram of PBAT and PCL is attributed to PBAT, as Monteiro *et al.*[30] previously verified. For PBAT/PCL/IBU-20, a crystalline pattern is observed due to the presence of peaks corresponding to PCL and IBU. For PBAT/PCL/IBU-30, on the other hand, the presence of broad and diffuse maxima observes an amorphization of IBU and PCL. Panda *et al.*[31] also observed the amorphization of IBU in an electrospun polyvinylpyrrolidone (PVP) system and highlighted this as a favorable point for better solubility of the drug. Celebioglu and Uyar[32] also observed the formation of entirely amorphous IBU in hydroxypropyl-beta-cyclodextrin membranes with increasing IBU concentration.

DSC analysis was used to evaluate the possibility of changes in the crystallinity of the ibuprofen films (Figure 5). All values of temperatures and heat (melting and crystallization) obtained by TA-50WS are presented in Table 2. The DSC curves show that endothermic peak 1 is related to PCL and the aliphatic monomer of PBAT.[14]
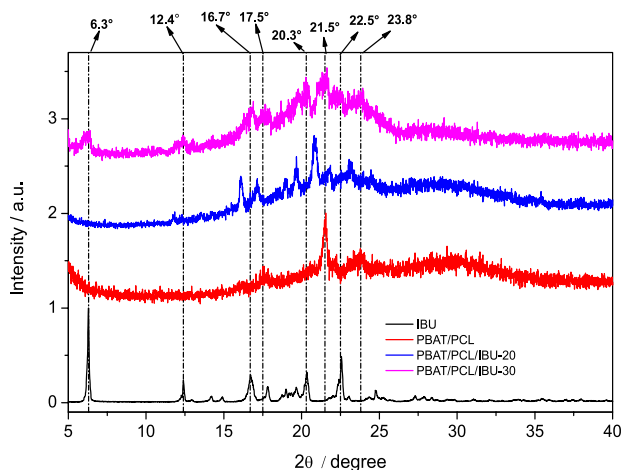
Figure 4. X-ray diffractograms for IBU (black), PBAT/PCL (red), PBAT/PCL/IBU-20 (blue), and PBAT/PCL/IBU-30 (pink).

Endothermic peak 2, present in PBAT/PCL/IBU-30, refers to the crystalline phase of β-form crystals of butylene adipate (BA) present in PBAT.[33] The appearance of peak 2 indicates that IBU acts as an agent that causes a fusion-refusion mechanism, causing a β-to-α transition of the BA segment to occur.[34] Finally, exothermic peak 3 is related to the aromatic monomer of PBAT melting,[14] while peak 4 is related to polymer recrystallization.[35]

First, it is observed that the incorporation and IBU concentration in PBAT/PCL films changes its $T_{melting}$ and

$\Delta H_{melting}$ for peak 1, mainly for 20% of IBU. For example, the incorporation of 20% of IBU increases the $\Delta H_{melting}$ about 15.4 J g^{-1} (from 21.6 to 37.0 J g^{-1}, respectively). It strongly indicates a greater polymeric organization (a higher crystallinity) under this condition. Additionally, the absence of the melting peak of IBU (peak 2) was observed in this film, indicating the overlap between the melting peak of IBU and PCL polymer.[36]

The event related to the PBAT monomer peak (peak 3) shows a considerable difference in the comparison between PBAT/PCL and PBAT/PCL/IBU films for both IBU concentrations. This decrease in the melting temperature with the IBU incorporation indicates the interaction between the drug and PBAT.[37] The polymer recrystallization peak (peak 4) temperatures vary from 71 to 76 ºC. The observation of the $\Delta H_{recrystalization}$ reveals a lower value to the greater IBU concentration (30% m m^{-1}), indicating less crystallization in this condition. This can be confirmed by the analysis of the crystallinity degree for films, calculated using equation 1 (Table 3).

The results in Table 3 reveal that increasing the IBU concentration from 20 to 30% (m m^{-1}) makes the film more plastic. These data agree with mechanical analyses that demonstrate the plasticizing characteristic of IBU. Furthermore, the reduction in crystallinity of the peak corroborates the XRD data that show the amorphization
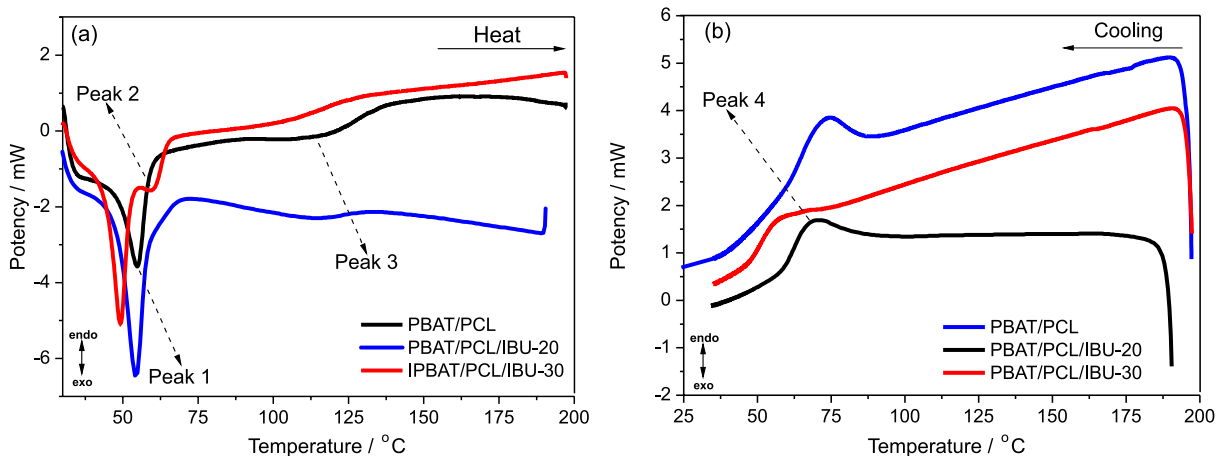

Figure 5. DSC curves under (a) heat and (b) cooling of PBAT/PCL films without and with IBU incorporation at different concentrations (20 and 30% m m^{-1}).

Table 2. Melting and recrystallization heat temperatures of PBAT/PCL films with and without IBU incorporation at different concentrations

Sample	Peak 1		Peak 2		Peak 3		Peak 4	
	$T_{melting}$ / ºC	ΔH_m / (J g^{-1})	$T_{melting}$ / ºC	ΔH_m / (J g^{-1})	$T_{melting}$ / ºC	ΔH_m / (J g^{-1})	$T_{crystallization}$ / ºC	$\Delta H_{recrystalization}$ / (J g^{-1})
PBAT/PCL	55	21.6	–	–	143	11.5	75	−17.7
PBAT/PCL/IBU-20	54	37.0	–	–	114	7.6	71	−16.1
PBAT/PCL/IBU-30	49	19.4	59	2.3	129	5.5	76	−6.9

$T_{melting}$: melting temperature, $T_{crystallization}$: crystallization temperature; $\Delta H_{recrystalization}$: recrystallization enthalpy; ΔH_m: melting enthalpy.

Table 3. Crystallinity degree calculated (equation 1) for the two peaks of the polymers melting containing IBU

| Sample	Crystallinity peak 1 / %	Crystallinity peak 3 / %
PBAT/PCL	28.1	25.6
PBAT/PCL/IBU-20	38.0	20.8
PBAT/PCL/IBU-30	18.9	10.9

PBAT: poly(butylene-adipate-*co*-terephthalate); PCL: poly-(ε-caprolactone); IBU: ibuprofen.

of the polymer and drug groups. Furthermore, when comparing the PCL (peak 1) and PBAT (peak 3) peaks, the more pronounced reduction in crystallinity for PBAT indicates a more significant interaction of IBU with this polymer. This fact also explains the greater crystallinity for PCL when compared to PBAT with the addition of IBU. The interaction of IBU with PBAT provides greater chain mobility for PCL[23] and, consequently, increases the volumetric amount of organized lamellas.

The analysis of degradation temperature is essential in developing a formulation for transdermal purposes. For example, it is necessary to evaluate if the sample suffers any thermal degradation in the skin temperature.[38] This can lead to premature drug delivery, compromising the matrice for this application. Figure 6 presents the thermogravimetric curves obtained by TGA analysis for the films.

First, IBU presents a total degradation in the temperature range from 150 to 240 ºC. The PBAT/PCL films show two stages of mass loss. The first is around 359 ºC (7.0% of loss mass), and the second is at 408 ºC (93% of loss change). This result is similar to results obtained by other researchers. It is related to the dehydration of hydroxyl groups of PLA and carboxylic groups of PBAT, the cleavage of ester linkage by hydrolysis, and C–O and C–C binding scission.[39,40] The thermograms of PBAT/PCL/IBU presented different degradation temperature ranges. The film
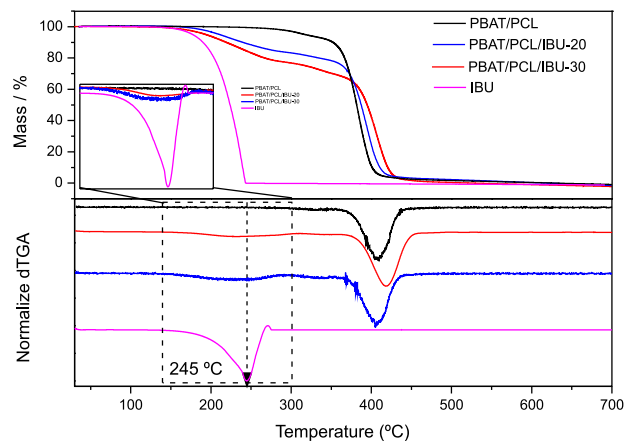

Figure 6. Thermogravimetric curves of IBU, PBAT/PCL, PBAT/PCL/IBU-20 and PBAT/PCL/IBU-30.

PBAT/PCL/IBU-20 showed a degradation range from 152 to 306 ºC, while for the film with higher IBU concentration, the final degradation temperature was 290 ºC.

These results corroborate the previous crystallinity degree studies, which revealed that PBAT/PCL/IBU-20 presents higher crystallinity (Table 3). It generates more significant intermolecular interactions between the polymeric chain, producing higher energy to promote film degradation. Finally, the results reveal that PBAT/PCL/IBU films presented thermal stability for biomedical purposes.[41]

The results presented here are similar to those obtained by us with the addition of silver sulfadiazine.[4] An increase in the crystallinity of PBAT/PCL films upon incorporation of the drug was observed. The results from this previous work and our current article show that regardless of the degree of drug polarity, there is an increase in polymer chain organization following the drug incorporation process.

Contact angle measurements were performed to evaluate the temporal wettability of the films containing or without IBU incorporated (Figure 7). It is known that low contact angles (< 90º) are related to the excellent wettability
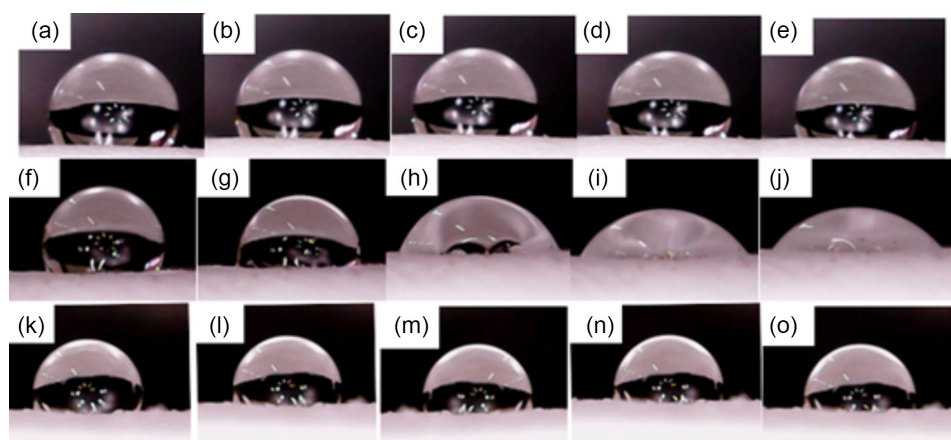
Figure 7. Contact angle images of PBAT/PCL (a-e), PBAT/PCL/IBU-20 (f-j), and PBAT/PCL/IBU-30 (k-o) at different times: 0 s (a, f, k); 120 s (b, g l); 240 s (c, h, m); 360 s (d, i, n), and 480 s (e, j, o).

(more hydrophilic behavior) of the films.[42] Table 4 presents the contact angle values for the images obtained in Figure 7.

Table 4. Contact angle values for wettability studies images reported in Figure 7

time / s	Contact angle / degree		
	PBAT/PCL	PBAT/PCL/IBU-20	PBAT/PCL/IBU-30
0	110	82	101
120	108	89	95
240	107	61	92
360	106	55	91
480	106	51	91

PBAT: poly(butylene-adipate-*co*-terephthalate); PCL: poly-(ε-caprolactone); IBU: ibuprofen.

It is necessary to mention that PBAT/PCL/IBU films presented lower contact angles than PBAT/PCL samples. This is an indication that IBU incorporation increases the hydrophilicity of the films. The films without IBU present hydrophobic behavior. The hydrophilicity is more pronounced by the film containing the lower IBU concentration (PBAT/PCL 20% (m m^{-1}) IBU). These data are in accordance with the mechanical analysis performed, probably indicating different localization of IBU in the films. For the film containing higher IBU concentration, part of the IBU molecules can be grafted into the PBAT/PCL chains, acting as a plasticizer. On the other hand, in the PBAT/PCL/IBU-20, the drug is located more externally, promoting increased wettability.

Figure 8 presents the percentage of IBU released *versus* time in PBS (pH 7.4) media.

First, the saturation in the liberation occurred in 840 min for both films studied. The saturation in the release curves occurred with the release of 64 and 58% of IBU for PBAT/PCL/IBU-20 and PBAT/PCL/IBU-30, respectively. The
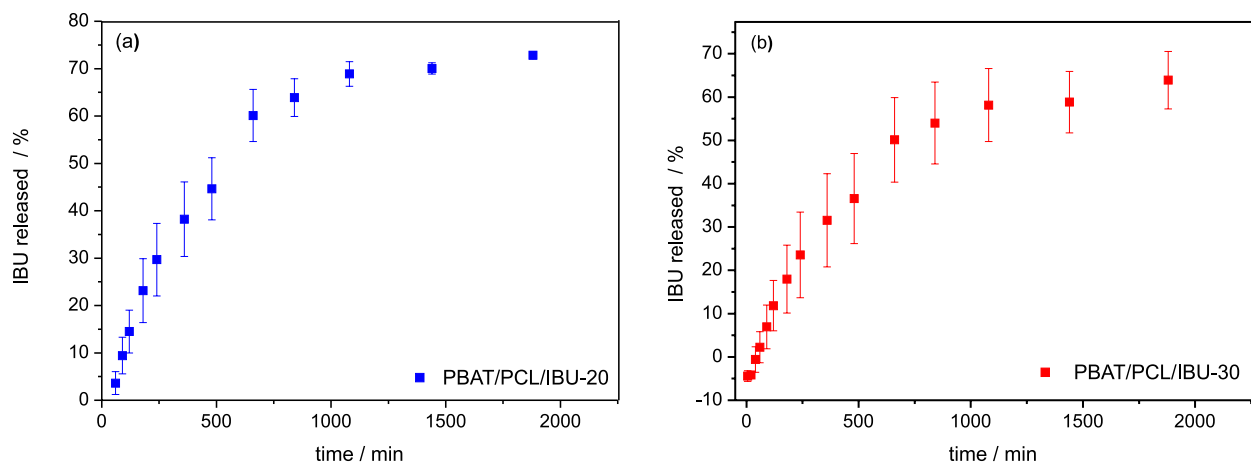
bead's film homogeneity in size verified in SEM analysis (Figure 1) for IBU concentrations justifies the continuum release until the maximum drug release is reached. However, it is demonstrated that a slower release of IBU for the film containing the higher IBU concentration (30% m m^{-1}). These results corroborate the assessment that in this film, a proportion of IBU is more internalized, making it more difficult for IBU to release.

The fitting of the experimental data according to several mathematic models of drug dissolution revealed the mechanism involved in the IBU release. The fitting graphs are present in the Supplementary Information (SI) section (Figure S1).

Table 5 presents the mathematical models used for the fitting.

The better model, according to the correlation coefficient values closest to one (R^2 = 1.0000), lower AIC, and greater models selection criterion (MSC), was Gompertz, independently of the IBU concentration in the films (Table 6).

Gompertz is applied with drug release profiles with great solubility and intermediary release rate.[53] This model describes a sharp increase during the onset of release and slowly converges to the asymptotic maximum release. Equation 13 presents the factors α and β, where the first is a parameter related to the non-dissolved drug proportion at a time equal to 1.[54] The β parameter describes the shape and dissolution rate. These values were α = 78.74 and β = 1.71 for PBAT/PCL/IBU-20 and α = 58.26, β = 1.48 for PBAT/PCL/IBU-30. The lower values obtained for the film with greater IBU concentration are according to the previously reported results, which showed a greater internalization of IBU in this film.[54]

PBAT/PCL films incorporated with the hydrophobic drug silver sulfadiazine presented a different release mechanism.

Figure 8. Percentage of IBU released in the function of the time for the films (a) PBAT/PCL/IBU-20, and (b) PBAT/PCL/IBU-30 in PBS (pH 7.4) at 37 ºC. The initial IBU concentration in films was 10 mg. The analysis was performed in quadruplicate.

Table 5. Mathematical models used to the fitting of liberation data of IBU from films

No.	Model	Equation	
1	zero-order[43]	$F = k_0 t$	(2)
2	first-order[44]	$F = 100 \times \left(1 - e^{-k_1 \times t}\right)$	(3)
3	Higuchi[45]	$F = k_H \times t^{\frac{1}{2}}$	(4)
4	Korsmeyer-Peppas[46]	$F = k_{HP} \times t^n$	(5)
5	Hixson-Crowell[47]	$F = 100 \times \left[1 - \left(1 - k_{HC} \times t\right)^3\right]$	(6)
6	Hopfenberg[48]	$F = 100 \times \left[1 - \left(1 - k_{HB} \times t\right)^n\right]$	(7)
7	Baker-Londsale[49]	$\frac{3}{2}\left[1 - \left(-\frac{F}{100}\right)^{\left(\frac{2}{3}\right)}\right] - \frac{F}{100} = k_{BL} \times t$	(8)
8	Peppas-Sahlin[50]	$F = k_1 \times t^m + k_2 \times t^{2m}$	(9)
9	quadratic[51]	$F = 100 \times \left(k_{1q} \times t^2 + k_2 \times t\right)$	(10)
10	Weibull[51]	$F = 100 \times \left[1 - e^{-\left(\frac{(t - T_i)^\beta}{\alpha}\right)}\right]$	(11)
11	logistic[48]	$F = F_{max} \frac{e^{\alpha_l + \beta_l \times \log t}}{1 + e^{\alpha_l + \beta_l \times \log t}}$	(12)
12	Gompertz[52]	$F = 100 \times e^{-\alpha_G \times e^{-\beta_G \times \log t}}$	(13)
13	Probit[52]	$F = 100 \times \phi\left[\alpha_P + \beta_P \times \log t\right]$	(14)

F: fraction (%) of drug released at time t; k_0: zero-order release constant; k_1: first order release constant; F_{max}: maximum fraction of drug released at infinite time; k_H: Higuchi release constant; k_{KP}: release constant incorporating structural and geometric characteristics of the drug-dose form; n: diffusion exponent (Korsmeyer-Peppas); k_{HC}: release constant in the Hixson-Crowell model; k_{HB}: combination constant in the Hopfenberg model; k_{BL}: constant in the Baker-Lonsdal model; k_{1q}: constant in the quadratic model; k_2: constant in the quadratic model denoting the relative contribution of t-dependent drug release (quadratic); α: scale parameter that defines the time scale of the process; β: shape parameter that characterizes the curve as exponential; Ti: localization parameter that represents the latency time before the start of the dissolution or release process; α_l: scale factor in the logistics 1 model; β_l: form factor in the logistics model; α_G: scale factor in the Gompertz model; β_G: form factor in Gompertz models; Φ: standard normal distribution; α_P: scale factor in the Probit model; β_P: form factor in the Probit model.

In these films, there are two steps in the release. The first was related to a non-Fickian mechanism ($0.75 < n < 1$) and a Fickian mechanism in the second ($0.35 < n < 0.75$).[4] The first step is related to a polymeric relaxation rate, followed by the second, where the dissolution of the drug in the dissolution medium was determinant. These results reveal that drug polarity degree is an essential factor in the release process from PBAT/PCL films.[4]

PBAT/PCL/IBU films were characterized after the IBU-controlled release process by SEM images (Figure 9).

The micrographs reveal the presence of a cluster around the beads, which disappeared after the release process. These clusters are probably the IBU molecules, which are the majority on the surface of films, leading to a faster release, as previously reported in this article.

FTIR (Figure S2, SI section) and TGA results (Figure S3, SI section) revealed that IBU was released from the fibers. The IR spectroscopy results showed a decrease or disappearance of prominent IBU bands in the films. For example, the band at 779 cm^{-1} related to the angular deformation of the hydrogen bond linked to the *para*-substituted aromatic ring of IBU disappeared after the release process (Figure S2). At the same time, the thermograms revealed a reduction in the intensity of mass change in the temperatures of IBU degradation (Figure S3).

After the IBU release process, the films showed thermal performance observed to understand more about possible morphological and structural changes in the polymer matrices (Figure 10). Table 7 presents the melting and recrystallization heat temperatures of PBAT/PCL/IBU films after release.

Comparison between the ΔH_m of samples containing IBU before (Table 2) and after the release process (Table 7) reveals a significant difference between both data. These data can indicate changes in the polymeric chain organization after the IBU release. This statement can be proved by crystallinity degree values obtained by the samples after IBU release (Table 8).

Table 8, when compared to Table 2, reveals an increase in the crystallinity of the films after the release of IBU. The significant increase in crystallinity, especially for PBAT, can be explained by the release of IBU. The release of IBU provides more freedom for the chains to diffuse into the already-formed lamellae, increasing their size and thus increasing the crystallinity of the sample.

Finally, the present article reveals the applicability of using PBAT/PCL films for the controlled release of the hydrophilic anti-inflammatory drug IBU. As previously mentioned, other articles of our research group also demonstrated the possibility of incorporating a hydrophobic antimicrobial agent, silver sulfonamide, in the same materials.[4] In this way, our future perspectives involve the association of IBU and silver sulfonamide in the same material to achieve a synergetic effect of anti-pathogenic and anti-inflammatory material for wound dressing. The final material would be more efficient in the treatment of several wounds. Several research groups have demonstrated the efficiency of hybrid materials of this nature. For example, recently, Alizadeh *et al.*[55] revealed the higher wound dressing potential nanofibers constituted of the antimicrobial polysaccharide chitosan with poly(vinyl

Table 6. Correlation coefficient (R), adjusted correlation coefficient (R²$_{adjusted}$), Akaike information criterion (AIC), and Models selection criterion (MSC) involving the fitting of release from PBAT/PCL films with different IBU concentrations

No.	PBAT/PCL/IBU-20				PBAT/PCL/IBU-30			
	R	R²$_{adjusted}$	AIC	MSC	R	R²$_{adjusted}$	AIC	MSC
1	0.8946	0.6982	122.4827	0.8317	0.8946	0.6982	122.4827	0.8377
2	0.9777	0.9379	99.1857	2.3908	0.9750	0.9231	96.5913	2.2590
3	0.9672	0.9095	105.8293	1.9479	0.9724	0.9101	100.6593	1.9878
4	0.9329	0.2321	123.9153	0.7422	0.9322	0.7614	115.0649	1.0274
5	0.9649	0.8961	106.8625	1.8790	0.9641	0.8818	102.7245	1.8501
6	0.9701	0.9056	106.5677	1.8987	0.9654	0.8919	102.6904	1.8524
7	0.9780	0.8865	108.8024	1.7497	0.9795	0.8825	103.5942	1.7921
8	0.9707	0.8999	109.0456	1.7335	0.9723	0.9109	102.2305	1.8830
9	0.9871	0.9687	87.0104	3.2025	0.9879	0.9687	83.9381	3.1025
10	0.9698	0.8976	103.8963	2.0768	0.9717	0.9187	100.9320	1.9696
11	0.9838	0.9517	89.3786	3.0446	0.9851	0.9649	87.4208	2.8703
12	0.9954	0.9888	73.6122	4.0957	0.9960	0.9913	65.7426	4.3155
13	0.9889	0.9705	84.3001	3.3832	0.9899	0.9772	80.7771	3.3132

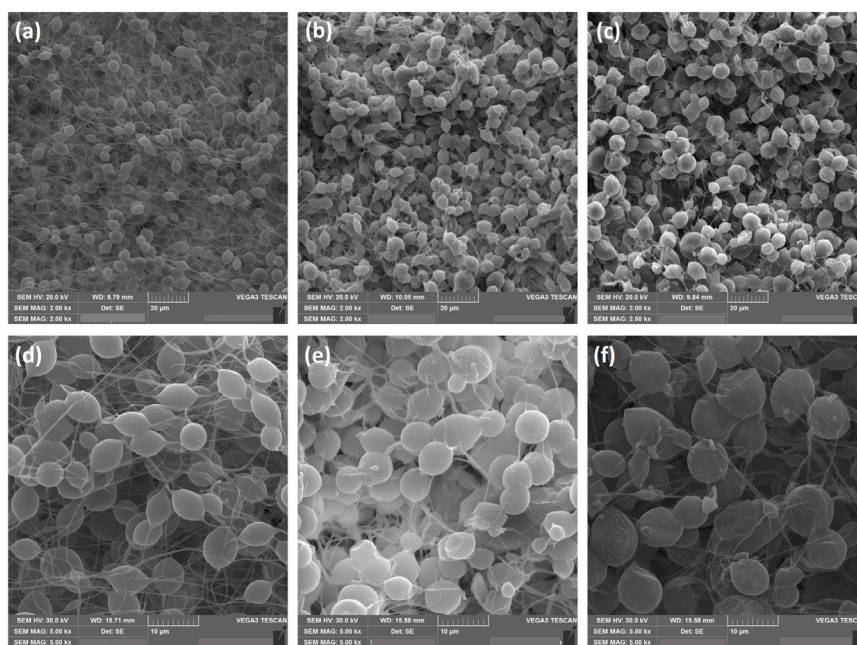PBAT: poly(butylene-adipate-*co*-terephthalate); PCL: poly-(ε-caprolactone); IBU: ibuprofen.

Figure 9. SEM micrographs of PBAT/PCL/IBU-20 film in the amplification of (a) 2000K×. PBAT/PCL/IBU-20 films after the release process (1500 min) in the amplification of (b) 2000K×, and (c) 5000K×; PBAT/PCL/IBU-30 films in the amplification of (d) 2000K×, and PBAT/PCL-IBU-30 after the release process (1500 min) in the amplification of (e) 2000K×, and (f) 5000K×.

alcohol) for the controlled release of antibiotics.[55] The final material presented superior protection and antibacterial effect than the isolated starting materials.[55]

Conclusions

The electrospinning technique was used to develop fibers of PCL and PBAT incorporating the anti-inflammatory drug IBU. We performed the obtention of fibers with different IBU concentrations (0, 20, and 30% m m^{-1}). Our results revealed that PBAT/PCL films presented different morphology and mechanical behavior after IBU incorporation. For example, fibers without IBU were continuous and uniform, while IBU caused bead formation. The mechanical analysis reveals that IBU incorporation decreased the tensile strength. The results also revealed a greater crystallinity (higher chain organization) for the films containing the lower IBU concentration (20%). Thermal
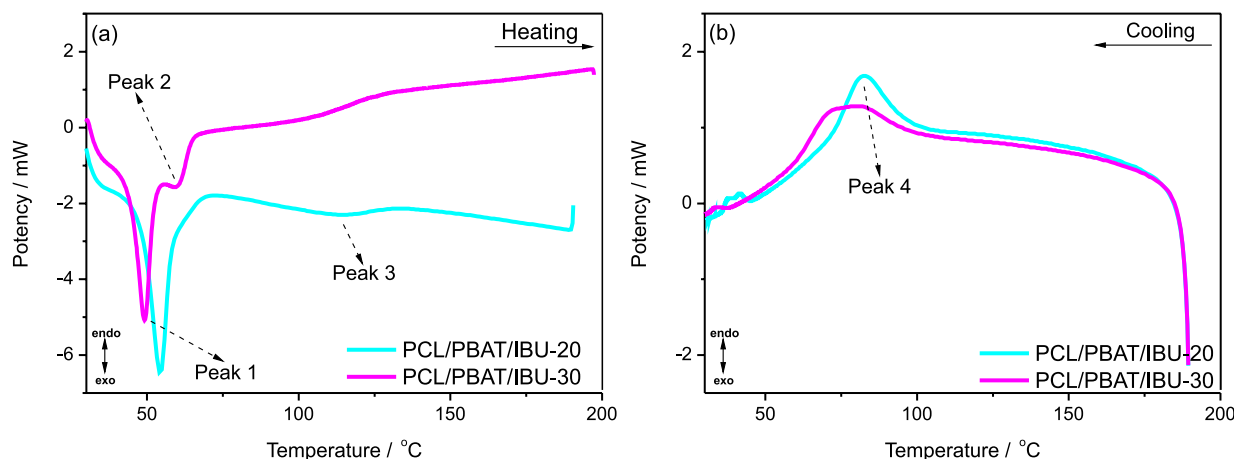
Figure 10. Thermogram of (a) heating and (b) cooling of PBAT/PCL/IBU films after IBU controlled release process (1500 min).

Table 7. Melting and recrystallization heat temperatures of PBAT/PCL/IBU films after the release process (1500 min)

Sample	Peak 1		Peak 2		Peak 3		Peak 4	
	$T_{melting}$ / °C	ΔH_m / (J g^{-1})	$T_{melting}$ / °C	ΔH_m / (J g^{-1})	$T_{melting}$ / °C	ΔH_m / (J g^{-1})	$T_{crystallization}$ / °C	$\Delta H_{recrystalization}$ / (J g^{-1})
PBAT/PCL	55	21.6	–	–	143	11.5	75	−17.7
PBAT/PCL/IBU-20	59	22.9	–	–	124	9.3	82	−25.9
PBAT/PCL/IBU-30	57	20.1	75	1.8	93	3.0	80	−17.4

$T_{melting}$: melting temperature; $T_{crystallization}$: crystallization temperature; $\Delta H_{recrystalization}$: recrystallization enthalpy; ΔH_m: melting enthalpy; PBAT: poly(butylene-adipate-*co*-terephthalate); PCL: poly-(ε-caprolactone); IBU: ibuprofen.

Table 8. Crystallinity percentage calculated for the two peaks of the polymers melting after IBU release (1500 min)

Sample	Crystallinity peak 1 / %	Crystallinity peak 3 / %
PBAT/PCL	28.1	25.6
PBAT/PCL/IBU-20 released	35.0	30.8
PBAT/PCL/IBU-30 released	26.9	16.8

PBAT: poly(butylene-adipate-*co*-terephthalate); PCL: poly-(ε-caprolactone); IBU: ibuprofen.

analysis revealed that PBAT/PCL/IBU films presented thermal stability. Contact angle measurements showed that IBU incorporation increased the films' hydrophilicity, and IBU is probably located more externally on fibers in PBAT/PCL 20% films. Controlled release studies indicated that IBU release from fibers obeys the Gompertz model and a polymeric reorganization after the drug release. All the results make it possible to use PBAT/PCL/IBU films for wound dressing.

Supplementary Information

Supplementary data are available free of charge at http://jbcs.sbq.org.br as PDF file.

Author Contributions

Janice C. Hardt was responsible for writing original draft, and data curation; Gabriel N. Fraga for investigation, and validation; Alessandra R. Medeiros for formal analysis, and data curation; Ariane R. S. Rossin for writing original draft, and writing-review; Josiane Caetano for investigation, and project administration; Matheus C. O. Leite for validation, and data curation; Bruno V. L. da Fonseca for validation, and conceptualization; Bruno H. Vilsinski for writing original draft, project administration and writing-review; Douglas C. Dragunski for project administration, visualization and resources.

References

1. Abioye, A. O.; Issah, S.; Kola-Mustapha, A. T.; *Int. J. Pharm.* **2015**, *490*, 112. [Crossref]

2. Das, S.; Subuddhi, U.; *J. Pharm. Anal.* **2019**, *9*, 108. [Crossref]

3. Rehman, F.; Ahmed, K.; Rahim, A.; Muhammad, N.; Tariq, S.; Azhar, U.; Khan, A. J.; us Sama, Z.; Volpe, P. L. O.; Airoldi, C.; *J. Mol. Liq.* **2018**, *258*, 319. [Crossref]

4. Hardt, J. C.; Pellá, M. C. G.; Reis Meira, A. C.; Rosenberger, A. G.; Caetano, J.; Dragunski, D. C.; *J. Mol. Liq.* **2021**, *339*, 116694. [Crossref]

5. Ozturk, E. A.; Ege, Z. R.; Murat, S.; Erdemir, G.; Kuruca, S.; Erkmen, Z. E.; Duygulu, O.; Gunduz, O.; Caykara, T.; Eroglu, M. S.; *Int. J. Biol. Macromol.* **2022**, *217*, 562. [Crossref]

6. Cheng, J.; Jun, Y.; Qin, J.; Lee, S.-H.; *Biomaterials* **2017**, *114*, 121. [Crossref]

7. Sun, Y.; Zhou, L.; Ding, Y.; Liu, C.; Mao, Z.; Jiang, Q.; Chen, J.; Chen, F.; Cao, Y.; *Talanta* **2024**, *266*, 125127. [Crossref]

8. Canales, D. A.; Reyes, F.; Saavedra, M.; Peponi, L.; Leonés, A.; Palza, H.; Boccaccini, A. R.; Grünewald, A.; Zapata, P. A.; *Int. J. Biol. Macromol.* **2022**, *210*, 324. [Crossref]

9. Aversa, C.; Barletta, M.; Cappiello, G.; Gisario, A.; *Eur. Polym. J.* **2022**, *173*, 111304. [Crossref]

10. Tadele, D. T.; Trinh, B. M.; Mekonnen, T. H.; *Polymer* **2023**, *283*, 126258. [Crossref]

11. Wang, Y.; Liu, Y.; Qian, Y.; Lv, L.; Li, X.; Liu, Y.; *Surf. Interfaces* **2022**, *28*, 101661. [Crossref]

12. Liu, Y.-Y.; Blazquez, J. P. F.; Yin, G.-Z.; Wang, D.-Y.; Llorca, J.; Echeverry-Rendón, M.; *Eur. Polym. J.* **2023**, *198*, 112388. [Crossref]

13. Rizvi, H. R.; D'Souza, N.; Ayre, B.; Ramesh, D.; *Emergent Mater.* **2019**, *2*,127. [Crossref]

14. Zanella, H. G.; Rossin, A. R. S.; Hardt, J. C.; Rosenberger, A. G.; Wiggers, J. C.; Caetano, J.; Dragunski, D. C.; *Quim. Nova* **2021**, *44*, 1245. [Crossref]

15. Louvis, A. R.; Silva, N. A. A.; *Rev. Virtual Quim.* **2016**, *8*, 1764. [Crossref]

16. ASTM-D882-12: *Standard Test Method for Tensile Properties of Thin Plastic Sheeting*, West Conshohocken, 2018.

17. Zhang, Y.; Huo, M.; Zhou, J.; Zou, A.; Li, W.; Yao, C.; Xie, S.; *AAPS J.* **2010**, *12*, 263. [Crossref]

18. Akaike, H.; *IEEE Trans. Autom. Control* **1974**, *19*, 716. [Crossref]

19. Costa, P.; Sousa Lobo, J. M.; *Eur. J. Pharm. Sci.* **2001**, *13*, 123. [Crossref]

20. Boggara, M. B.; Faraone, A.; Krishnamoorti, R.; *J. Phys. Chem. B* **2010**, *114*, 8061. [Crossref]

21. Sequeira, R. S.; Miguel, S. P.; Cabral, C. S. D.; Moreira, A. F.; Ferreira, P.; Correia, I. J.; *Int. J. Pharm.* **2019**, *570*, 118640. [Crossref]

22. Khan, I. A.; Anjum, K.; Ali, M. S.; Din, K.; *Colloids Surf., B* **2011**, *88*, 72. [Crossref]

23. Aho, J.; Edinger, M.; Botker, J.; Baldursdottir, S.; Rantanen, J.; *J. Pharm. Sci.* **2016**, *105*, 160. [Crossref]

24. Ibrahim, H. M.; Klingner, A.; *Polym. Test.* **2020**, *90*, 106647. [Crossref]

25. Lemraski, E. G.; Alibeigi, S.; Abbasi, Z.; *Mater. Today Commun.* **2022**, *33*, 104311. [Crossref]

26. Wiranidchapong, C.; Ruangpayungsak, N.; Suwattanasuk, P.; Shuwisitkul, D.; Tanvichien, S.; *Drug Dev. Ind. Pharm.* **2015**, *41*, 1037. [Crossref]

27. Wadaugsorn, K.; Panrong, T.; Wongphan, P.; Harnkarnsujarit, N.; *Ind. Crops Prod.* **2022**, *176*, 114311. [Crossref]

28. Jin, G.; Li, Y.; Prabhakaran, M. P.; Tian, W.; Ramakrishna, S.; *J. Bioact. Compat. Polym.* **2014**, *29*, 628. [Crossref]

29. Yu, D.-G.; Shen, X.-X.; Branford-White, C.; White, K.; Zhu, L.-M.; Annie Bligh, S. W.; *Nanotechnology* **2009**, *20*, 055104. [Crossref]

30. Monteiro, M. S. S. B.; Lunz, J.; Sebastião, P. J.; Tavares, M. I. B.; *Mater. Sci. Appl.* **2016**, *7*, 680 [Crossref]

31. Panda, D. S.; Alruwaili, N. K.; Swain, K.; Pattnaik, S.; *Acta Chim. Slovaca* **2022**, *69*, 483. [Crossref]

32. Celebioglu, A.; Uyar, T.; *Mol. Pharmaceutics* **2019**, *16*, 4387. [Crossref]

33. Gan, Z.; Kuwabara, K.; Yamamoto, M.; Abe, H.; Doi, Y.; *Polym. Degrad. Stab.* **2004**, *83*, 289. [Crossref]

34. Yang, J.; Chen, Y.; Qin, S.; Liu, J.; Bi, C.; Liang, R.; Dong, T.; Feng, X.; *Ind. Eng. Chem. Res.* **2015**, *54*, 8048. [Crossref]

35. Rossin, A. R. S.; Caetano, J.; Zanella, H. G.; Baccatti, R. A.; Gaffo, L.; Muniz, E. C.; Caetano, W.; Stolf, S. F.; Dragunski, D. C.; *J. Therm. Anal. Calorim.* **2022**, *147*, 4579. [Crossref]

36. Andrioli, A.; Prado, L. D.; da Costa, M. A.; Rocha, H. V. A.; *Rev. Cienc. Farm. Basica Apl.* **2014**, *35*, 401. [Crossref]

37. Arruda, L. C.; Magaton, M.; Bretas, R. E. S.; Ueki, M. M.; *Polym. Test.* **2015**, *43*, 27. [Crossref]

38. Talebi, N.; Lopes, D.; Lopes, J.; Macário-Soares, A.; Dan, A. K.; Ghanbari, R.; Kahkesh, K. H.; Peixoto, D.; Giram, P. S.; Raza, F.; Veiga, F.; Sharifi, E.; Hamishehkar, H.; Paiva-Santos, A. C.; *Appl. Mater. Today* **2023**, *30*, 101726. [Crossref]

39. Kerman, I.; Toppare, L.; Yilmaz, F.; Yagci, Y.; *J. Macromol. Sci., Part A: Pure Appl. Chem.* **2005**, *42*, 509. [Crossref]

40. Kumar, M.; Mohanty, S.; Nayak, S. K.; Rahail Parvaiz, M.; *Bioresour. Technol.* **2010**, *101*, 8406. [Crossref]

41. Vilsinski, B. H.; Souza, P. R.; de Oliveira, A. C.; Filho, C. M. C.; Valente, A. J. M.; Muniz, E. C.; Borges, O.; Gerola, A. P.; Caetano, W.; Martins, A. F.; *Mater. Today Commun.* **2020**, *26*, 101889. [Crossref]

42. Rbihi, S.; Aboulouard, A.; Laallam, L.; Jouaiti, A.; *Surf. Interfaces* **2020**, *21*, 100708. [Crossref]

43. Gurny, R.; Doelker, E.; Peppas, N. A.; *Biomaterials* **1982**, *3*, 27. [Crossref]

44. Polli, J. E.; Rekhi, G. S.; Augsburger, L. L.; Shah, V. P.; *J. Pharm. Sci.* **1997**, *86*, 690. [Crossref]

45. Higuchi, T.; *J. Pharm. Sci.* **1961**, *50*, 874. [Crossref]

46. Korsmeyer, R. W.; Gurny, R.; Doelker, E.; Buri, P.; Peppas, N. A.; *Int. J. Pharm.* **1983**, *15*, 25. [Crossref]

47. Hixson, A. W.; Crowell, J. H.; *Ind. Eng. Chem.* **1931**, *23*, 923. [Crossref]

48. Enscore, D. J.; Hopfenberg, H. B.; Stannett, V. T.; *Polymer* **1977**, *18*, 793. [Crossref]

49. Baker, M. I.; Walsh, S. P.; Schwartz, Z.; Boyan, B. D.; *J. Biomed. Mater. Res., Part B* **2012**, *100*, 1451. [Crossref]

50. Peppas, N. A.; Sahlin, J. J.; *Int. J. Pharm.* **1989**, *57*, 169. [Crossref]

51. Paarakh, M. P.; Jose, P. A.; Setty, C.; Peterchristoper, G. V.; *Int. J. Pharm. Res. Technol.* **2019**, *8*, 12. [Crossref]

52. Tsong, Y.; Hammerstrom, T.; Chen, J. J.; *J. Biopharm. Stat.* **1997**, *7*, 423. [Crossref]

53. Siepmann, J.; Siepmann, F.; *Int. J. Pharm.* **2013**, *453*, 12. [Crossref]

54. Khan, M. A.; Shafeeq, T.; *J. Sci. Res.* **2009**, *1*, 539. [Crossref]

55. Alizadeh, S.; Farshi, P.; Farahmandian, N.; Ahovan, Z. A.; Hashemi, A.; Majidi, M.; Azadbakht, A.; Darestanifarahani, M.; Sepehr, K. S.; Kundu, S. C.; Gholipourmalekabadi, M.; *Int. J. Biol. Macromol.* **2023**, *229*, 22. [Crossref]

J. Braz. Chem. Soc. **2024**, *35,* 7, e-20240004

13 of 13